Chemical Engineering Science 66 (2011) 6272–6279

Contents lists available at SciVerse ScienceDirect

Chemical Engineering Science

journal homepage: www.elsevier.com/locate/ces

Effects of wall-heating on the linear instability characteristics of pressure-driven two-layer channel flow

V.T.S.R. Kumar Reddy, Vinod M. Janardhanan, Kirti Chandra Sahu *

Department of Chemical Engineering, Indian Institute of Technology Hyderabad, Yeddumailaram 502 205, Andhra Pradesh, India

ARTICLE INFO

Article history:
Received 23 February 2011
Received in revised form
1 July 2011
Accepted 2 September 2011
Available online 14 September 2011

Keywords:
Multiphase flow
Hydrodynamics
Stability
Interface
Isothermal
Laminar flow

ABSTRACT

The linear stability analysis of a pressure-driven two-layer channel flow of two immiscible, Newtonian and incompressible fluids is considered. The walls of the channel are maintained at different constant temperatures and Nahme's law is applied to model the temperature dependence of the fluid viscosity. A modified Orr–Sommerfeld equation for the disturbance streamfunction coupled to a linearized energy equation is derived and solved using a spectral collocation method. Our results indicate that increasing the dimensionless top wall temperature has a non-monotonic effect on the linear stability characteristics. We also found that increasing the thermal conductivity and density ratios stabilise the flow for the set of parameter values considered; the viscosity ratio has a non-monotonic effect on the maximal growth rate. An energy 'budget' analysis shows that the most dangerous mode is of 'interfacial' type.

1. Introduction

Two-fluid flows are common in many practical applications, such as, the cleaning of first-moving consumer goods plants, transportation of crude oil in pipelines (Joseph et al., 1997), mixing of liquids using centerline injectors, up-stream of static mixers (Cao et al., 2003), and the removal of highly viscous or elasto-viscoplastic material adhering to pipes by using fast-flowing water streams (Regner et al., 2007). The instabilities of immiscible two-fluid Poiseuille flows in isothermal systems have been addressed by many authors via asymptotic (Yih, 1967; Yiantsios and Higgins, 1988a; Khomami, 1990a, 1990b) and linear stability analyses (Yiantsios and Higgins, 1988b; Hooper and Boyd, 1983; Boomkamp and Miesen, 1996; South and Hooper, 1999; Frigaard, 2001; Sahu et al., 2007; Sahu and Matar, 2010b), as well as experimental techniques (Kao and Park, 1972).

The origin of the study of the interfacial instability is the early work of Yih (1967), who considered the stability of two-fluid flow to two-dimensional long-wave disturbances. Yih used an asymptotic analysis to derive an expression for the complex wave speed as a function of the relevant system parameters such as the density, viscosity and thickness ratios. He then demonstrated that instability exists due to an interfacial mode which results from a viscosity stratification even in the limit of vanishingly small Reynolds numbers. The appearance of a shear mode, which corresponds to a short-wave Tollmien–Schlichting mode at sufficiently large Reynolds numbers was first shown numerically by Yiantsios and Higgins (1988b). They (Yiantsios and Higgins, 1988a) also studied the effects of gravity and interfacial tension via an asymptotic analysis using the perturbation scheme of Hooper and Boyd (1983). The latter authors examined the short-wave asymptotic of the interfacial instability between two unbounded viscous fluids. They provided predictions of critical Reynolds numbers for both the shear and interfacial modes and demonstrated the existence of discrepancies between these predictions and the experimental data of Kao and Park (1972). They also compared their results with the weakly nonlinear evolution of the interface considered by Hooper and Grimshaw (1985).

Recently, Sahu et al. (2007) studied the linear instability of two-dimensional disturbances in a pressure-driven two-layer channel flow, wherein a Newtonian fluid layer overlies a layer of a Herschel–Bulkley fluid. Their results indicate that increasing the yield stress, prior to the formation of unyielded zones, and shear-thickening tendency are destabilising. The convective and absolute nature of two-dimensional disturbances in a similar system was studied by Valluri et al. (2010). The effect of three-dimensional disturbances on the linear stability characteristics was also studied by Sahu and Matar (2010b). Frigaard (2001) studied the two-dimensional linear stability of two-layer Poiseuille flow of two Bingham fluids. Unlike in the study of Sahu et al. (2007), the case studied by Frigaard (2001), involves an unyielded region between the Newtonian fluid and the yielded

* Corresponding author.
E-mail address: ksahu@iith.ac.in (K.C. Sahu).

0009-2509/$ - see front matter © 2011 Elsevier Ltd. All rights reserved.
doi:10.1016/j.ces.2011.09.003

part of the Bingham fluid. Interfacial waves would not develop under such conditions; this suppression of interfacial modes then leads to super-stable two-layer flows Frigaard (2001).

We briefly review the linear stability analyses of single fluid channel flow with wall heating. In case single fluid flow through channel, Potter and Graber (1972) and Pinarbasi and Liakopoulos (1995) found that the temperature difference between the walls is always destabilising. Later, Schäfer and Herwig (1993) confirmed this finding by conducting an asymptotic analysis of a similar problem. Unlike the above studies, Wall and Wilson (1996) and Sameen and Govindarajan (2007) rescaled the governing equations using the viscosity of the fluid at the hot wall, and the average viscosity across the channel, respectively. Their results, in contradiction to these in Potter and Graber (1972), and Schäfer and Herwig (1993) indicate that the temperature difference between the walls is stabilising. Sameen and Govindarajan (2007) also studied the effect of buoyancy and found that the Poiseuille–Rayleigh–Bénard mode which appears at a moderate Grashof number, merged with the Poiseuille mode at high Grashof number. Carriere and Monkewitz (1999) showed that the flow is absolutely unstable at very low Reynolds numbers and high Grashof numbers. Recently, Sahu and Matar (2010a) performed a linear stability analysis to study the effects of viscous heating on Poiseuille flow in an asymmetrically heated channel and found that viscous heating has a destabilising influence.

Non-isothermal flow of two immiscible Newtonian fluids in a channel with different wall temperature was studied by Pinarbasi (2002) via linear stability and long wave asymptotic analyses. Considering silicon/water and oil/water systems, they found that depending on the disturbance wavenumber and height of the interface the temperature difference of the walls can stabilise or destabilise the flow, unlike the case of singe-layer flows. They also found that for intermediate and large wavenumber the surface tension has a stabilising influence. They obtained stable flow region by heating the flow from the bottom and for particular surface tension. Although this work is the closest to the present work, their study is limited only to very low Reynolds number and small temperature difference. As the working fluids in their study are fixed, they considered only two typical viscosity ratios. Also density stratification was not considered in their paper. In contrast the present study is general. The detailed study of the effects of viscosity and density stratifications at high Reynolds number is investigated in the present work. We have conducted an energy 'budget' analysis to study the physics of this problem.

As the above brief review shows, except the study of Pinarbasi (2002) the work carried out on two-fluid immiscible channel flows has so far been for isothermal systems only. Yet, thermal gradients can potentially have a drastic effect on the flow dynamics due to their influence on the viscosity. This has been the subject of the present work; we study the effects of temperature gradient on the linear stability characteristics. To the best of our knowledge, the effects of thermal gradient on the linear stability characteristics of two-layer immiscible flow has not been studied previously. The rest of this paper is organised as follows. Details of the problem formulation are provided in Section 2, and the results of the linear stability analysis are presented in Section 3. Concluding remarks are provided in Section 4.

2. Formulation

We consider a pressure-driven channel flow of two immiscible Newtonian and incompressible fluids. The walls are maintained at different constant temperatures, such that, T_l and T_u represent the temperatures at the bottom and top walls, respectively; $\Delta T \equiv T_u - T_l$. The density and thermal conductivity of both the fluids are assumed to be constant; (ρ_1, κ_1) and (ρ_2, κ_2) are the density and thermal conductivity of the lower and upper fluids, respectively. A rectangular coordinate system, (x, y), is used to model this flow where x and y denote the streamwise and wall normal coordinates, respectively, as shown in Fig. 1. The rigid and impermeable channel walls are located at $y=0$ and $y=H$, respectively, and the sharp interface, which separates the immiscible fluids, is at $y=h^0$. The following Nahme-type viscosity–temperature relationship (Sukanek et al., 1973; Nahme, 1940; Pinarbasi and Ozalp, 2001; Sahu and Matar, 2010b) is used that approximates the variation of viscosity of the lower (μ_1) and upper (μ_2) fluids, respectively:

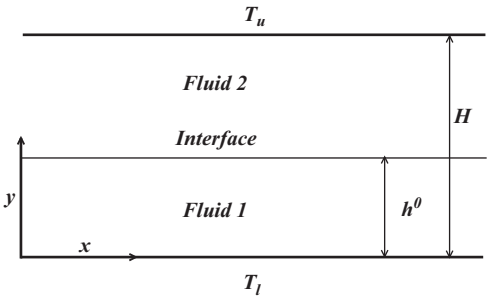

Fig. 1. Schematic of a two-layer flow in a channel of height H, where h^0 represents the thickness of the lower layer.

$$\mu_1(T) = \mu_1(T_l)\exp\left[-\frac{\beta(T-T_l)}{T_l}\right], \quad \mu_2(T) = \mu_2(T_l)\exp\left[-\frac{\beta(T-T_l)}{T_l}\right], \tag{1}$$

where T_l has been choosen as a reference temperature; β is a dimensionless activation energy parameter that stands for the sensitivity of the viscosity to temperature variation; for liquids, β is a positive number, and we restrict ourselves to this case. $\mu_1(T_l)$ and $\mu_2(T_l)$ are the viscosities of the lower and upper fluids, respectively, at temperature T_l. The height of the channel, H, and the maximum velocity, U_m, are used as the length and velocity scales in order to non-dimensionalise the equations of motion. The viscosity is scaled with $\mu_2(T_l)$; density and heat conduction coefficient are normalised with those of the upper fluid, respectively. As buoyancy is known to play a negligible role on the instability of such flows (Sameen and Govindarajan, 2007), we have neglected this effect in the present study. The reduced dimensionless pressure $\tilde{p}_i$ in fluid 'i' is related to the corresponding total dimensional pressure p_i through

$$\tilde{p}_i = \frac{H}{\mu_l U_m}[p_i + \rho_i g(y-h^0)] \quad (i=1,2), \tag{2}$$

where g is the gravitational acceleration. The following scaling is used to non-dimensionalise the temperature in both the layers:

$$T_i = \frac{\tilde{T}_i T_l}{\beta} + T_l, \tag{3}$$

where tildes designate dimensionless quantities. After dropping tildes, the dimensionless form of the viscosity–temperature relationships of both the fluids are given by

$$\mu_1 = m\exp(-T_1) \quad \text{and} \quad \mu_2 = \exp(-T_2), \tag{4}$$

where $m(\equiv \mu_1(T_l)/\mu_2(T_l))$ is the viscosity ratio. The various dimensionless parameters appearing in the governing equations are the dimensionless gravitational parameter, $G(\equiv(\rho_1-\rho_2)gH^2/\mu_2(T_l)U_m)$, the Reynolds number, $Re(\equiv\rho_2 U_m H/\mu_2(T_l))$, the Prandtl number, $Pr(\equiv c_p\mu_2(T_l)/\kappa_2)$ and the inverse capillary number, $\Gamma(\equiv\gamma/\mu_2(T_l)U_m)$, in which γ denotes the interfacial tension. The governing dimensionless equations are given in the Appendix A.

2.1. Base state

The base state whose linear stability characteristics will be analyzed, corresponds to a steady, parallel, fully developed flow in both the layers separated by a flat interface i.e, $V_i=0$; U_i and T_i^0 are only a function of y and pressure distribution ($P_1=P_2=P$) is linear in x:

$$T_1^0 = c_1 y + c_2, \tag{5}$$

$$T_2^0 = c_3 y + c_4, \tag{6}$$

$$U_1 = \frac{1}{mc_1}\left(\frac{dP}{dx}y + c_5\right)e^{c_1 y} - \frac{1}{mc_1^2}\frac{dP}{dx}e^{c_1 y} + c_6, \tag{7}$$

$$U_2 = \frac{1}{c_3}\left(\frac{dP}{dx}y + c_7\right)e^{[c_3(y-1)+r_T]} - \frac{1}{c_3^2}\frac{dP}{dx}e^{[c_3(y-1)+r_T]} + c_8. \tag{8}$$

The subscripts '1' and '2' are used to represent quantities associated with the lower and upper fluids, respectively. We obtain Eqs. (5)–(8) by integrating the steady, fully developed dimensionless Navier–Stokes and energy equations (given in Appendix A), imposing the fixed temperature and no-slip velocity conditions at the walls and demanding continuity of velocity, temperature and the tangential component of the stress at the interface. The integration constants are given by

$$c_1 = r_T/[\kappa_r + h^0(1-\kappa_r)], \quad c_2 = 0, \quad c_3 = c_1\kappa_r \quad \text{and} \quad c_4 = r_T - c_3. \tag{9}$$

$$c_5 = c_7 = \frac{\dfrac{dP}{dx}\left[\dfrac{e^{c_1 h^0}}{c_1}\left(\dfrac{1}{c_1}-h^0\right) + \dfrac{e^{[c_3(h^0-1)+r_T]}}{c_3}\left(h^0-\dfrac{1}{c_3}\right) + \dfrac{e^{r_T}}{c_3}\left(\dfrac{1}{c_3}-1\right) - \dfrac{1}{mc_1^2}\right]}{\dfrac{1}{mc_1}(e^{c_1 h^0}-1) + \dfrac{e^{r_T}}{c_3}(1-e^{[c_3(h^0-1)]})}, \tag{10}$$

$$c_6 = \frac{1}{mc_1^2}\left(\frac{dP}{dx} - c_1 c_5\right), \quad c_8 = \frac{e^{r_T}}{c_3^2}\left[\frac{dP}{dx}(1-c_3) - c_5 c_3\right], \tag{11}$$

where $r_T(\equiv\beta(T_u-T_l)/T_l)$ and $\kappa_r(\equiv\kappa_1/\kappa_2)$ are the dimensionless top wall temperature and thermal conductivity ratio, respectively. Typical basic state profiles of the steady, fully developed streamwise velocity component and temperature for different values of m and r_T are shown in Fig. 2. The rest of the parameter values are $Re=100$, $Pr=1$, $G=0$, $\Gamma=0$ and $\kappa_r=1.1$. Inspection of Fig. 2(a) reveals that increasing the value of viscosity ratio, m, leads to a decrease in the gradient of velocity of the bottom fluid in the wall-normal direction at the interface; the temperature profile remains unaffected by this variation in m (see Fig. 2(b)). It can be seen in Fig. 2(c) that increasing r_T (which corresponds to the increase in the dimensionless top wall temperature) has a similar effect as that of viscosity ratio. The temperature profiles for different values of r_T can be seen in Fig. 2(d) as expected.

2.2. Linear stability analysis

We examine the linear stability of the base state, obtained by solving Eqs. (5)–(8), to infinitesimal, two-dimensional (2D) disturbances using a normal modes analysis. Each flow variable is expressed as the sum of a base state and a 2D perturbation,

$$(\tilde{u}_i,\tilde{v}_i,\tilde{p}_i,\tilde{T}_i,\tilde{\mu}_i)(x,y,t) = [U_i(y),0,P_i,T_i^0(y),\mu_i^0(y)] + (\hat{u}_i,\hat{v}_i,\hat{p}_i,\hat{T}_i,\hat{\mu}_i)(x,y,t), \tag{12}$$

with $i=1, 2$. Similarly h can be expressed as

$$h(x,y,t) = h^0 + \hat{h}, \tag{13}$$

where $\hat{u}$ and $\hat{v}$ denote the streamwise and wall-normal components of the perturbation velocity vector, respectively; $\hat{p}_i$ and $\hat{T}_i$ represent perturbation pressure and temperature, respectively; $\hat{\mu}_i=(d\mu_i^0/dT_i^0)\hat{T}_i$ represents the perturbation viscosity. The superscript '0' designates the base state quantities. Substitution of Eqs. (12) and (13) into the governing equations followed by subtraction of the base state equations, subsequent linearization and elimination of the pressure perturbation yields the linear

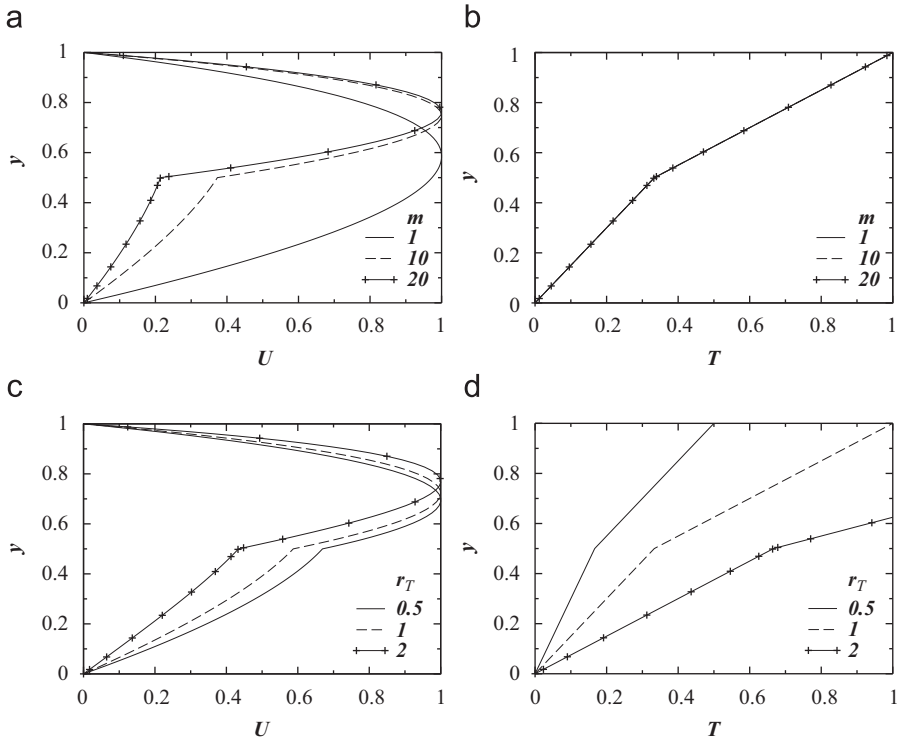

Fig. 2. The streamwise velocity and temperature profiles for different values of (a, b) m with $r_T=1$, and (c, d) r_T with $m=5$. The rest of the parameter values are $h^0=0.5$, $Re=100$, $Pr=1$, $G=0$, $\Gamma=0$ and $\kappa_r=2$.

stability equations in terms of primary variables. These equations are re-expressed in terms of the perturbation streamfunction, $[(\hat{u}_i,\hat{v}_i)\equiv\ \partial\hat{\psi}_i/\partial y,-\partial\hat{\psi}_i/\partial x]$, and then decomposed into an amplitude and a wave part by using a normal modes analysis:

$$(\hat{\psi}_i,\hat{p}_i,\hat{T}_i,\hat{\mu}_i)(x,y,t)=(\psi_i,p_i,T_i,\mu_i)(y)e^{\mathbf{i}(\alpha x-\omega t)},$$

$$\hat{h}(x,y,t)=\tilde{h}e^{i(\alpha x-\omega t)},\quad i=1,2, \tag{14}$$

where α and $\omega(\equiv\alpha c)$ denote the streamwise wavenumbers (real) and frequency (complex) of the disturbance, wherein c is a complex phase speed of the disturbance, such that, a given mode is unstable if $\omega_i>0$, stable if $\omega_i<0$ and neutrally stable if $\omega_i=0$ (Drazin and Reid, 1985; Schmid and Henningson, 2001). This yields the following stability equations inn both the layers.

In the lower layer:

$$\begin{aligned}\mathbf{i}\alpha rRe[(U_1-c)[\psi_1''-\alpha^2\psi_1]-U_1''\psi_1]&=\mu_1^0[\psi_1''''-2\alpha^2\psi_1''+\alpha^4\psi_1]\\&+2\mu_1^{0\prime}[\psi_1'''-\alpha^2\psi_1']+\mu_1^{0\prime\prime}[\psi_1''+\alpha^2\psi_1]\\&+\mu_1U_1'''+2\mu_1'U_1''+(\alpha^2\mu_1+\mu_1'')U_1',\end{aligned} \tag{15}$$

$$\mathbf{i}\alpha rRePr[(U_1-c)T_1-\psi_1T_1^{0\prime}]=\kappa_r[T_1''-\alpha^2T_1]. \tag{16}$$

In the upper layer:

$$\begin{aligned}\mathbf{i}\alpha Re[(U_2-c)[\psi_2''-\alpha^2\psi_2]-U_2''\psi_2]&=\mu_2^0[\psi_2''''-2\alpha^2\psi_2''+\alpha^4\psi_2]\\&+2\mu_2^{0\prime}[\psi_2'''-\alpha^2\psi_2']+\mu_2^{0\prime\prime}[\psi_2''+\alpha^2\psi_2]\\&+\mu_2U_2'''+2\mu_2'U_2''+(\alpha^2\mu_2+\mu_2'')U_2',\end{aligned} \tag{17}$$

$$\mathbf{i}\alpha RePr[(U_2-c)T_2-\psi_2T_2^{0\prime}]=[T_2''-\alpha^2T_2]. \tag{18}$$

These equations are then subject to the following boundary conditions: no-slip and no-penetration conditions at the walls can be written as

$$\psi_1'=\psi_1=0\quad\text{and}\quad T_1=0\text{ at }y=0, \tag{19}$$

$$\psi_2'=\psi_2=0\quad\text{and}\quad T_2=0\text{ at }y=1. \tag{20}$$

The kinematic boundary condition gives

$$h=\frac{\psi_1}{(c-U_1)}=\frac{\psi_2}{(c-U_2)}. \tag{21}$$

continuity of the temperature, the velocity components and of the normal and tangential stress components at the interface are expressed as

$$T_1+hT_1'=T_2+hT_2', \tag{22}$$

$$\psi_1'+hU_1'=\psi_2'+hU_2', \tag{23}$$

$$\psi_1=\psi_2, \tag{24}$$

$$T_2'=\kappa_rT_1', \tag{25}$$

$$\begin{aligned}&\mathbf{i}\alpha Re[r\{(c-U_1)\psi_1'+U_1'\psi_1\}-\{(c-U_2)\psi_2'+U_2'\psi_2\}]-3\alpha^2\mu_1^0\psi_1'+\mu_1^0\psi_1'''\\&+\mu_1^{0\prime}(\psi_1''+\alpha^2\psi_1)+\mu_1U_1''+\mu_1'U_1'+3\alpha^2\mu_2^0\psi_2'-\mu_2^0\psi_2'''\\&-\mu_2^{0\prime}(\psi_2''+\alpha^2\psi_2)-\mu_2U_2''-\mu_2'U_2'=\alpha^2(\Gamma\alpha^2+G)\frac{\psi_2'-\psi_1'}{\mathbf{i}\alpha(U_2'-U_1')},\end{aligned} \tag{26}$$

$$\mu_2^0(\psi_2''+\alpha^2\psi_2)=\mu_1^0(\psi_1''+\alpha^2\psi_1)+\mu_1U_1'-\mu_2U_2'-(\mu_1^0U_1''-\mu_2^0U_2'')\frac{\psi_1}{(c-U_1)}. \tag{27}$$

Here, $r(\equiv\rho_1/\rho_2)$ is the density ratio; prime represents differentiation with respect to y. Our stability equations and the boundary conditions match with those of Sahu and Matar (2010b) and Nouar et al. (2007) for Newtonian fluid under isothermal condition. We have confirmed that Eqs. (15)–(18) along with the boundary conditions (19)–(27) describe an eigenvalue problem where c is the eigenvalue, and (ψ_1, T_1) and (ψ_2, T_2) are the eigenfunctions corresponding to the intervals $[0-h^0]$ and $[h^0-1]$, respectively. The above procedure allows the numerical calculation of the dispersion relations $\omega_i=\omega_i(\alpha;Re,m,r,\Gamma,G)$. A similar technique had previously been used by Sahu et al. (2007) and Sahu and Matar (2010b). This eigenvalue problem is then solved using the public domain software, LAPACK, and the Chebyshev spectral collocation method (Canuto et al., 1987).

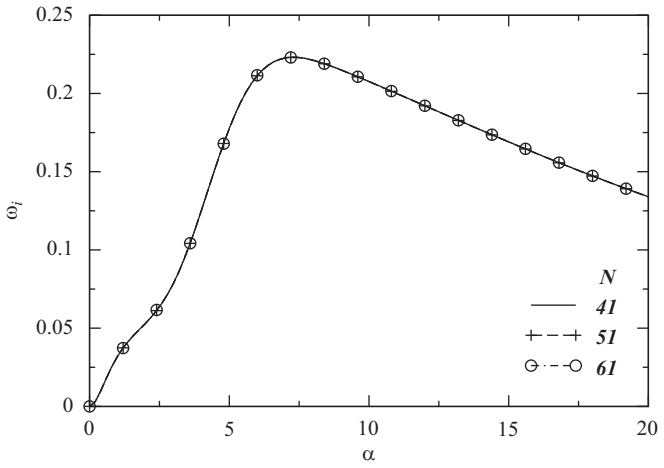

Fig. 3. The effect of increasing the order of Chebyshev polynomials in each layer, N, on the variation of growth rate (ω_i) with α. The rest of the parameter values are $Re=100$, $Pr=1$, $m=5$, $r=1.1$, $G=0$, $\Gamma=0$, $h^0=0.5$, $r_T=1$ and $\kappa_r=1.1$.

We checked the dependence of our numerical solutions upon mesh refinement by considering different values of the order of Chebyshev polynomials, N, in Fig. 3. The rest of the parameter values are $Re=100$, $Pr=1$, $m=5$, $r=1.1$, $G=0$, $\Gamma=0$, $h^0=0.5$, $r_T=1$ and $\kappa_r=1.1$. It can be seen that the results are indistinguishable for $N>41$; thus, $N=51$ is used to generate the rest of the results. Our results are also in excellent agreement with those of Sahu and Matar (2010b), South and Hooper (1999) and Yiantsios and Higgins (1988a) for isothermal flows.

3. Results and discussion

In this section, we discuss our linear stability results; particular attention will be given to the effects of varying r_T, κ_r, m and r on the linear stability characteristics since the influence of h^0 and Γ on the stability of two-layer flows has been well studied. An energy analysis is conducted in order to understand the mechanism and nature of this instability.

We investigate first the effect of varying the top wall temperature, r_T, on the linear stability characteristics. In Fig. 4, we plot numerically generated dispersion curves with the rest of the parameter values the same as those used to generate Fig. 3. The dispersion curves depicted in Fig. 4 are paraboloidal, and $\omega_i>0$ over a finite band of wavenumbers, indicating the presence of a linear instability; there are also well-defined 'most-dangerous' and 'cut-off' modes that correspond to the values of α for which ω_i is maximal and beyond which $\omega_i>0$, respectively. As shown in Fig. 4(a), increasing r_T for $h^0=0.5$ increases the maximal growth rate for $r_T<2$; a further increase in the value of r_T decreases the maximal growth rate. This non-monotonic effect can also be seen in the value of the wavenumber associated with the cut-off mode. A similar behaviour was observed by Pinarbasi (2002) in the silicon/water system. As discussed in the introduction section, depending on the reference viscosity used in case of single-layer

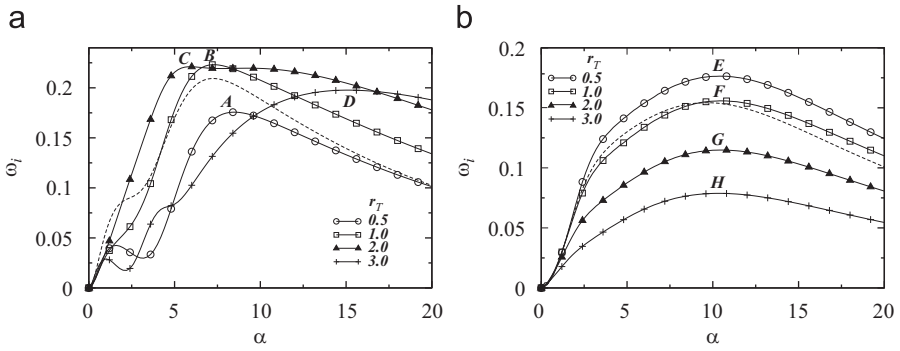

Fig. 4. Effect of varying the top wall temperature, r_T, on the dispersion curves (ω_i vs. α): (a) $h^0=0.5$ and (b) $h^0=0.2$. The rest of the parameter values are the same as those used to generate Fig. 3. The dotted lines show the dispersion curves obtained for an isothermal system ($r_T=0$).

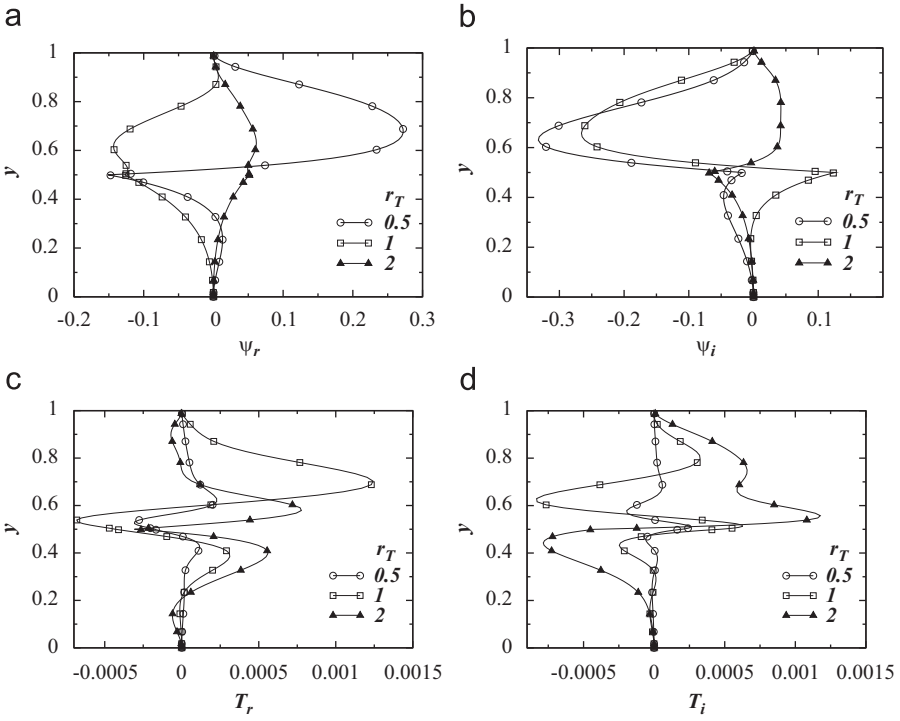

Fig. 5. The panels (a) and (b) show the real and imaginary parts of the disturbance stream-function, respectively. The real and imaginary parts of the temperature disturbance are shown in panels (c) and (d), respectively. The rest of the parameter values are $Re=100$, $Pr=1$, $m=5$, $r=1.1$, $G=0$, $\Gamma=0$ and $h^0=0.5$.

flows the temperature difference between the walls has monotonically stabilising (Wall and Wilson, 1996; Sameen and Govindarajan, 2007) or destabilising (Potter and Graber, 1972; Pinarbasi and Liakopoulos, 1995) effect on the stability characteristics. For $h^0=0.2$, increasing r_T decreases the maximal growth rate and the wavenumber associated with 'cut-off' mode; hence its effect is stabilising. In this case, the wavenumber associated with the 'most-dangerous' mode is almost the same for different r_T values considered. The dispersion curves correspond to an isothermal system ($r_T=0$) for the same set of parameters are shown by the dotted lines in Fig. 4(a) and (b) for reference.

Typical profiles of the real and imaginary parts of the disturbance eigenfunctions are shown in Fig. 5. The parameter values considered to generate this figure is the same as those used in Fig. 4. It can be seen that both the real and imaginary parts of the disturbance temperature (T_r and T_i) are maximum near the vicinity of the interface. It can also be seen that there is a sudden change in the gradient of the real and imaginary parts of the stream-function disturbance (ψ_r and ψ_i) at the interface of the fluids. All this effects predict the appearance of the interfacial

Table 1
Energy 'budgets' for the points labelled *A*, *B*, *C* and *D* in Fig. 4.

Point	REY_1	REY_2	DIS_1	DIS_2	*TAN*	*TEN*	*HYD*
A	−0.0378	0.2763	−2.2783	−7.9073	10.9471	0	0
B	−0.0394	0.4845	−1.9728	−6.9987	9.5264	0	0
C	−0.0199	1.1594	−2.3421	−8.9532	11.1558	0	0
D	−0.0052	0.0479	−0.5812	−4.4815	6.0199	0	0

Table 2
Energy 'budgets' for the points labelled *E*, *F*, *G* and *H* in Fig. 4.

Point	REY_1	REY_2	DIS_1	DIS_2	*TAN*	*TEN*	*HYD*
E	−0.0094	0.0684	−2.1082	−5.8309	8.8800	0	0
F	−0.0083	0.0506	−2.0034	−6.1619	9.1230	0	0
G	−0.0060	0.0106	−1.8020	−7.0215	9.8188	0	0
H	−0.0043	−0.0299	−1.6457	−8.3997	11.0796	0	0

instability. In order to understand the physical mechanism and the nature of unstable modes, we perform an energy budget analysis, similar to that given in Sahu et al. (2007), following the methodology outlined in the Appendix B. The energy 'budgets' associated with the points labelled *A*, *B*, *C* and *D* (the maxima in the dispersion curves for $h^0 = 0.5$) in Fig. 4(a) are given in Table 1. The figures in Table 1 represent the contribution arising from each term in Eq. (43) scaled by the total spatially averaged rate of change of disturbance kinetic energy, *KIN*.

The energy decomposition reveals that *TAN* (work done by the velocity and stress disturbances in the direction tangential to the interface) provides the largest positive contribution to *KIN*. Thus the unstable modes examined are all of the 'interfacial' type. The other positive, albeit smaller, contribution to *KIN* for this set of parameters is due to the Reynolds stress in the upper fluid, REY_2. The dissipative terms, DIS_1 and DIS_2 provide negative contributions; this indicates that viscous dissipation provides a restoring effect and is stabilising, as expected. It can also be seen that for this set of parameter values, REY_2 increases with increasing r_T, reaching to a minimum value for $r_T \approx 2$; a further increase in r_T values leads to a rapid decrease in REY_2. This may provide an explanation for the non-monotonic dependence on r_T shown in Fig. 4(a). The Reynolds stress term associated with the lower fluid, REY_1, makes a small negative contribution to *KIN*.

The energy 'budgets' associated with the points labelled *E*, *F*, *G* and *H* (the maxima in the dispersion curves for $h^0 = 0.2$) in Fig. 4(b) are given in Table 2. This energy decomposition reveals that the largest contribution to *KIN* is due to *TAN*, confirming the most dangerous mode to be of 'interfacial' type. It can be seen that increasing r_T decreases REY_2. This may be a possible reason because of which increasing the top wall temperature has a stabilising influence for the set of parameter values considered.

Next, we investigate the effect of varying the thermal conductivity ratio, κ_r, on the linear stability characteristics for $h^0 = 0.5$ and $h^0 = 0.2$ in Fig. 6(a) and (b), respectively. The rest of the parameter values are the same as those used to generate

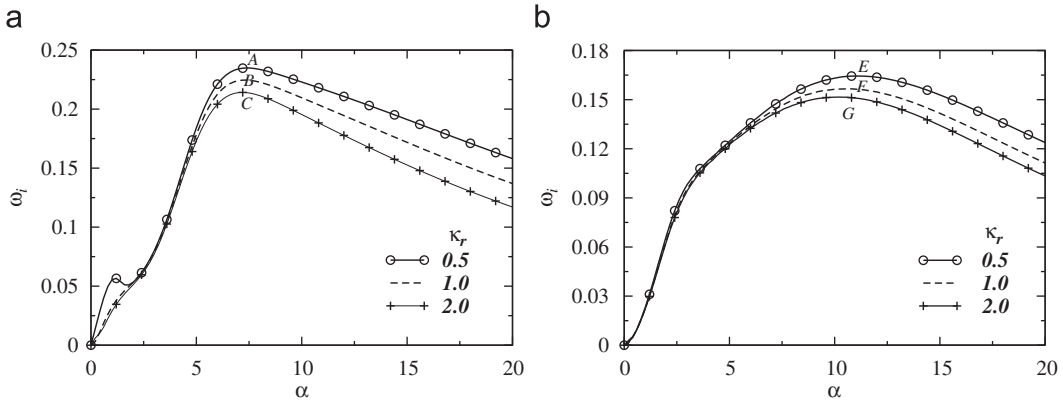

Fig. 6. Effect of varying the thermal conductivity ratio, κ_r, on the dispersion curves (ω_i vs. α): (a) $h^0 = 0.5$ and (b) $h^0 = 0.2$. The rest of the parameter values are the same as those used to generate Fig. 3.

Table 3
Energy 'budgets' for the points labelled *A*, *B*, *C*, *D* and *E* in Fig. 6.

Point	REY_1	REY_2	DIS_1	DIS_2	*TAN*	*TEN*	*HYD*
A	−0.0301	0.4223	−1.5894	−5.7196	7.9168	0	0
B	−0.0381	0.4759	−1.9142	−6.8006	9.2770	0	0
C	−0.0489	0.5551	−2.4225	−8.5576	11.4739	0	0
D	−0.0074	0.0525	−1.7365	−5.4280	8.1194	0	0
E	−0.0081	0.0450	−1.9540	−6.0640	8.9811	0	0
F	−0.0086	0.0455	−2.1466	−6.5865	9.6962	0	0

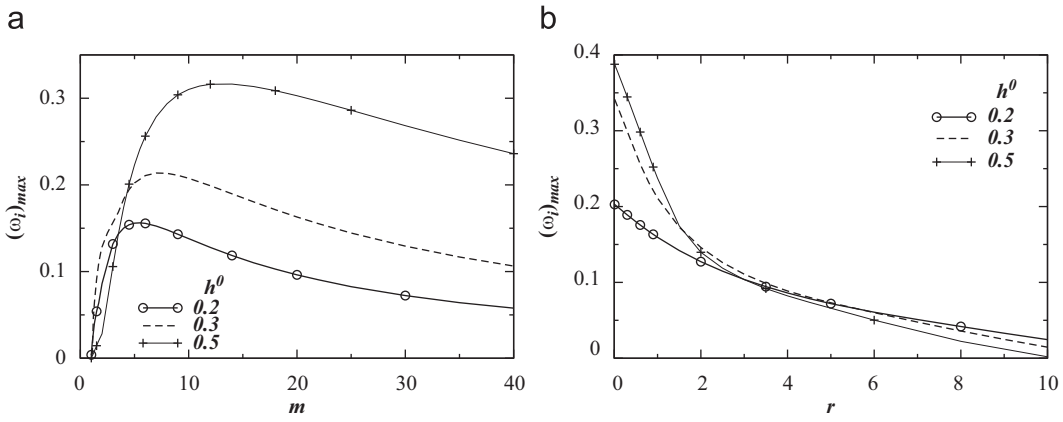

Fig. 7. Variation of $(\omega_i)_{max}$ with (a) the viscosity ratio, *m* (b) the density ratio, *r*. The unspecified parameter values in panels (a) and (b) are the same as those used to generate Fig. 3.

Fig. 3. It can be seen in Fig. 6(a) and (b) that increasing κ_r decreases the maximal growth rate and 'cut-off' wave number. The energy 'budgets' associated with the points labelled *A*, *B* and *C*, and *D*, *E* and *F* (the maxima in the dispersion curves in Fig. 6(a) and (b), respectively) are given in Table 3. This energy decomposition reveals that the unstable modes examined are all of the 'interfacial' type as *TAN* provides the largest positive contribution to *KIN*. It can be seen that although increasing κ_r increases REY_2 for labelled *A*, *B* and *C* and approximately constant for *D*, *E* and *F*, the negative contribution to *KIN* by the total dissipative energy (*DIS*) also increases rapidly. Thus increasing κ_r has overall a stabilising influence.

The effect of varying the viscosity and density ratios on the maximal growth rate, $(\omega_i)_{max}$, is examined in Fig. 7(a) and (b), respectively, for different values of h^0. It can be seen in Fig. 7(a) that $(\omega_i)_{max}$ increases with increasing the value of viscosity ratio, *m* and reaches to a maximum for an intermediate value of *m* for all h^0 considered. A further increase in *m*, however, leads to a decrease in the maximal growth rate. Close inspection of Fig. 7(a) also reveals that the viscosity ratio associated with the maximal growth rate increases with increasing h^0. The variation of $(\omega_i)_{max}$ with the density ratio, *r*, for different values of h^0 is shown in Fig. 7(b). It can be seen that $(\omega_i)_{max}$ decreases with increasing the value of *r* for this set of parameter values considered. In case of a pressure-driven two-layer channel flow with a Newtonian fluid layer overlying a layer of a Herschel-Bulkley fluid, Sahu et al. (2007) found a non-monotonic dependence on *r*.

4. Concluding remarks

We have investigated the linear instabilities in a pressure-driven two-layer channel flow of two immiscible Newtonian and incompressible fluids, wherein the channel walls are maintained at different constant temperatures. The viscosity–temperature dependence is modelled by a Nahme-type relationship. The modified Orr–Sommerfeld equation for the disturbance stream-function coupled to a linearized energy equation is derived and solved using a spectral collocation method. Our results indicate that increasing r_T, which corresponds to the increase in the dimensionless top wall temperature has a non-monotonic effect on the linear stability characteristics for $h^0=0.5$; increasing r_T promotes the instability for $r_T<2$, but has a stabilising influence for $r_T>2$. However, increasing r_T stabilises the flow for $h^0=0.2$. We also found that increasing the thermal conductivity and density ratios stabilise the flow for the set of parameter values considered. The viscosity ratio has a non-monotonic effect on the maximal growth rate. We also found (not shown) that surface tension has a stabilising influence. An energy 'budget' analysis shows that the most dangerous modes are 'interfacial' ones.

Acknowledgements

The authors would like to acknowledge the support of the Indian Institute of Technology Hyderabad, India.

Appendix A. Dimensionless governing equations

Without tildes decoration the dimensionless governing equations in both the layers are given by:

In the lower layer:

$$\frac{\partial u_1}{\partial x}+\frac{\partial v_1}{\partial y}=0, \tag{28}$$

$$rRe\left[\frac{\partial u_1}{\partial t}+u_1\frac{\partial u_1}{\partial x}+v_1\frac{\partial u_1}{\partial y}\right]=-\frac{\partial p_1}{\partial x}+\frac{\partial}{\partial x}\left[2\mu_1\frac{\partial u_1}{\partial x}\right]+\frac{\partial}{\partial y}\left[\mu_1\left(\frac{\partial u_1}{\partial y}+\frac{\partial v_1}{\partial x}\right)\right], \tag{29}$$

$$rRe\left[\frac{\partial v_1}{\partial t}+u_1\frac{\partial v_1}{\partial x}+v_1\frac{\partial v_1}{\partial y}\right]=-\frac{\partial p_1}{\partial y}+\frac{\partial}{\partial x}\left[\mu_1\left(\frac{\partial u_1}{\partial y}+\frac{\partial v_1}{\partial x}\right)\right]+\frac{\partial}{\partial y}\left[2\mu_1\frac{\partial v_1}{\partial y}\right], \tag{30}$$

$$rRePr\left[\frac{\partial T_1}{\partial t}+u_1\frac{\partial T_1}{\partial x}+v_1\frac{\partial T_1}{\partial y}\right]=\kappa_r\left[\frac{\partial^2 T_1}{\partial x^2}+\frac{\partial^2 T_1}{\partial y^2}\right]. \tag{31}$$

In the upper layer:

$$\frac{\partial u_2}{\partial x}+\frac{\partial v_2}{\partial y}=0, \tag{32}$$

$$Re\left[\frac{\partial u_2}{\partial t}+u_2\frac{\partial u_2}{\partial x}+v_2\frac{\partial u_2}{\partial y}\right]=-\frac{\partial p_2}{\partial x}+\frac{\partial}{\partial x}\left[2\mu_2\frac{\partial u_2}{\partial x}\right]+\frac{\partial}{\partial y}\left[\mu_2\left(\frac{\partial u_2}{\partial y}+\frac{\partial v_2}{\partial x}\right)\right], \tag{33}$$

$$Re\left[\frac{\partial v_2}{\partial t}+u_2\frac{\partial v_2}{\partial x}+v_2\frac{\partial v_2}{\partial y}\right]=-\frac{\partial p_2}{\partial y}+\frac{\partial}{\partial x}\left[\mu_2\left(\frac{\partial u_2}{\partial y}+\frac{\partial v_2}{\partial x}\right)\right]+\frac{\partial}{\partial y}\left[2\mu_2\frac{\partial v_2}{\partial y}\right], \tag{34}$$

$$RePr\left[\frac{\partial T_2}{\partial t}+u_2\frac{\partial T_2}{\partial x}+v_2\frac{\partial T_2}{\partial y}\right]=\left[\frac{\partial^2 T_2}{\partial x^2}+\frac{\partial^2 T_2}{\partial y^2}\right]. \tag{35}$$

The wall boundary conditions are

$$u_1=v_1=0 \quad \text{and} \quad T_1=0 \quad \text{at } y=0, \tag{36}$$

$$u_2=v_2=0 \quad \text{and} \quad T_2=r_T \quad \text{at } y=1. \tag{37}$$

Interfacial boundary conditions are

$$p_1-p_2+\frac{2\mu_2}{(1+h_x^2)}[v_{2y}+h_x^2u_{2x}-h_x(u_{2y}+v_{2x})]-\frac{2\mu_1}{(1+h_x^2)}[v_{1y}+h_x^2u_{1x}-h_x(u_{1y}+v_{1x})]=-\frac{\Gamma h_{xx}}{(1+h_x^2)^{\frac{3}{2}}}+Gh, \tag{38}$$

$$\mu_2[2h_x(v_{2y}-u_{2x})+(1-h_x^2)(u_{2y}+v_{2x})]-\mu_1[2h_x(v_{1y}-u_{1x})+(1-h_x^2)(u_{1y}+v_{1x})]=0. \tag{39}$$

The jump energy balance at the interface is given by

$$(T_{2y}-T_{2x}h_x)-\kappa_r(T_{1y}-T_{1x}h_x)=0, \tag{40}$$

and kinematic boundary condition is

$$h_t+uh_x=v.$$

Continuity of the velocity components and temperature at the interface:

$$u_1=u_2, \quad v_1=v_2 \quad \text{and} \quad T_1=T_2. \tag{41}$$

The dimensionless form of the viscosity–temperature relationship becomes

$$\mu_1=m\exp(-T_1) \quad \text{and} \quad \mu_2=\exp(-T_2). \tag{42}$$

Here, $r_T(\equiv\beta(T_u-T_l)/T_l)$ and $\kappa_r(\equiv\kappa_1/\kappa_2)$ are the dimensionless top wall temperature and thermal conductivity ratio, respectively; $m(\equiv\mu_1(T_l)/\mu_2(T_l))$ and $r(\equiv\rho_1/\rho_2)$ are the viscosity ratio at the reference temperature, T_l, and density ratio, respectively. The various dimensionless parameters appearing in the governing equations are the dimensionless gravitational parameter, $G(\equiv(\rho_1-\rho_2)gH^2/\mu_2(T_l)U_m)$, the Reynolds number, $Re(\equiv\rho_2U_mH/\ \mu_2(T_l))$, the Prandtl number, $Pr(\equiv c_p\mu_2(T_l)/\kappa_2)$ and the inverse capillary number, $\Gamma(\equiv\gamma/\mu_2(T_l)U_m)$.

Appendix B. Energy balance

We provide here a derivation of the energy equation given in Boomkamp and Miesen (1996), Sahu et al. (2007) and Sahu and Matar (2010b). Decomposition of this equation into energy production and dissipation terms allows one to isolate the mechanisms by which energy is transferred from the base flow to the disturbances. This decomposition also allows one to determine the type of instability mode, whether 'interfacial' or 'shear'.

The energy equation is derived by taking the inner product of the horizontal and vertical components of the Navier–Stokes equations with their respective velocity components. The resultant equation is then averaged over the wavelength, λ, and integrated over the height of channel. Application of this procedure to the equations in both fluids, addition of the resultant equations and making use of the Gauss-divergence theorem yields

$$\sum_{j=1}^{2} KIN_j = \sum_{j=1}^{2} DIS_j + \sum_{j=1}^{2} REY_j + INT, \tag{43}$$

where subscript $j=1$ and $j=2$ represent the lower and upper fluids, respectively. In Eq. (43), KIN_j, DIS_j and REY_j are expressed by

$$KIN_j = \frac{r_j}{\lambda}\frac{\mathrm{d}}{\mathrm{d}t}\int_{a_j}^{b_j} \mathrm{d}y \int_0^{\lambda} \mathrm{d}x \left[\frac{1}{2}(\hat{u}_j^2 + \hat{v}_j^2)\right], \tag{44}$$

$$DIS_j = -\frac{1}{\lambda Re}\int_{a_j}^{b_j} dy \int_0^{\lambda} \mu_j \, \mathrm{d}x \left[2\left(\frac{\partial \hat{u}_j}{\partial x}\right)^2 + \left(\frac{\partial \hat{u}_j}{\partial y} + \frac{\partial \hat{v}_j}{\partial x}\right)^2 + 2\left(\frac{\partial \hat{v}_j}{\partial y}\right)^2\right], \tag{45}$$

$$REY_j = \frac{r_j}{\lambda}\int_{a_j}^{b_j} \mathrm{d}y \int_0^{\lambda} \mathrm{d}x \left[-\hat{u}_j \hat{v}_j \frac{\partial U_j}{\partial y}\right]; \tag{46}$$

for the lower fluid, $r_1 = r$, $a_1 = 0$, $b_1 = h^0$ and for the upper fluid, $r_2 = 1$, $a_2 = h^0$, $b_2 = 1$. KIN_j represents the spatially averaged rate of change of disturbance kinetic energy and is proportional to the growth rate. DIS_j represents the viscous dissipation of energy and is always negative; note the presence of μ_j inside the integrand as it is a function of local temperature across the channel. REY_j represents energy production ('Reynolds stress') term. Physically, *DIS* is associated the energy transfer from the disturbance to the meanflow; thus always has a stabilising influence. On the other hand, *REY* is responsible for the energy transfer from the meanflow to the disturbance, hence positive value of *REY* is destabilising. $INT = NOR + TAN$ is associated with the existence of an interface and is decomposed into *NOR* and *TAN*, the work done by the velocity and stress disturbances in the directions normal and tangential to the interface, respectively. *NOR* is given by

$$NOR = \frac{1}{\lambda Re}\int_0^{\lambda} [\hat{v}_1 \tau_1^{yy} - \hat{v}_2 \tau_2^{yy}]_h \, \mathrm{d}x, \tag{47}$$

which is further decomposed into *TEN* and *HYD*, work done against the deformation of the interface due to interfacial tension and gravity, respectively:

$$NOR \equiv TEN + HYD = \frac{1}{\lambda Re}\int_0^{\lambda} [\hat{v}\Gamma\hat{\eta}_{xx}]_{y=h} \, \mathrm{d}x + \frac{1}{\lambda Re}\int_0^{\lambda} [\hat{v}G\hat{\eta}]_{y=h} \, \mathrm{d}x. \tag{48}$$

TAN, is given by

$$TAN = \frac{1}{\lambda Re}\int_0^{\lambda} [u_1 \tau_1^{xy} - u_2 \tau_2^{xy}]_h \, \mathrm{d}x. \tag{49}$$

In Eqs. (47) and (49), the components of stress tensor are defined as

$$\tau_j^{xy} = \mu_j\left(\frac{\partial u_j}{\partial y} + \frac{\partial v_j}{\partial x}\right) \quad \text{and} \quad \tau_j^{yy} = -p_j + 2\mu_j \frac{\partial v_j}{\partial y}, \tag{50}$$

where p_j denote the pressure disturbance.

References

Boomkamp, P.A.M., Miesen, R.H.M., 1996. Classification of instabilities in parallel two-phase flow. Int. J. Multiphase Flow 22, 67.

Canuto, C., Hussaini, M.Y., Quarteroni, A., Zang, T., 1987. Spectral Methods in Fluid Dynamicsfirst ed. Springer-Verlag, Amsterdam.

Cao, Q., Ventresca, L., Sreenivas, K.R., Prasad, A.K., 2003. Instability due to viscosity stratification downstream of a centreline injector. Can. J. Chem. Eng. 81, 913.

Carriere, P., Monkewitz, P., 1999. Convective versus absolute instability in mixed Rayleigh–Benard–Poiseuille convection. J. Fluid Mech. 384, 243–262.

Drazin, P.G., Reid, W.H., 1985. Hydrodynamic StabilityCambridge University Press, Cambridge.

Frigaard, I.A., 2001. Super-stable parallel flows of multiple visco-plastic fluids. J. Non-Newt. Fluid Mech. 100, 49–76.

Hooper, A.P., Boyd, W.G.C., 1983. Shear flow instability at the interface between two fluids. J. Fluid Mech. 128, 507.

Hooper, A.P., Grimshaw, R., 1985. Nonlinear instability at the interface between two viscous fluids. Phys. Fluids 28, 37–45.

Joseph, D.D., Bai, R., Chen, K.P., Renardy, Y.Y., 1997. Core-annular flows. Ann. Rev. Fluid Mech. 29, 65.

Kao, T.W., Park, C., 1972. Experimental investigations of the stability of channel flows. Part 2. Two-layered co-current flow in a rectangular channel. J. Fluid Mech. 52, 401–423.

Khomami, B., 1990a. Interfacial stability and deformation of two stratified power-law fluids in plane Poisuille flow. Part I. Stability analysis. J. Non-Newt. Fluid Mech. 36, 289–303.

Khomami, B., 1990b. Interfacial stability and deformation of two stratified power-law fluids in plane Poisuille flow. Part II. Interface deformation. J. Non-Newt. Fluid Mech. 37, 19–36.

Nahme, R., 1940. Beiträge zur hydrodynamischen theorie der lagerreibung. Ingenieur Arch. 11, 191–209.

Nouar, C., Kabouya, N., Dusek, J., Mamou, M., 2007. Modal and non-modal linear stability of the plane Bingham–Poiseuille flow. J. Fluid Mech. 577, 211–239.

Pinarbasi, A., 2002. Interface stabilization in two-layer channel flow by surface heating or cooling. Eur. J. Mech. B/Fluids 21, 225–236.

Pinarbasi, A., Liakopoulos, A., 1995. Role of variable viscosity in the stability of channel flow. Int. Comm. Heat Mass Transfer 22, 837–847.

Pinarbasi, A., Ozalp, C., 2001. Effect of viscosity models on the stability of a non-Newtonian fluid in a channel with heat transfer. Int. Comm. Heat Mass Transfer 28 (3), 369–378.

Potter, M.C., Graber, E., 1972. Stability of plane Poiseuille flow with heat transfer. Phys. Fluids 15 (3), 387–391.

Regner, M., Henningsson, M., Wiklund, J., Östergren, K., Trägårdh, C., 2007. Predicting the displacement of yoghurt by water in a pipe using CFD. Chem. Eng. Technol. 30, 844–853.

Sahu, K.C., Matar, O.K., 2010a. Stability of plane channel flow with viscous heating. J. Fluids Eng. 132, 011202.

Sahu, K.C., Matar, O.K., 2010b. Three-dimensional linear instability in pressure-driven two-layer channel flow of a Newtonian and a Herschel–Bulkley fluid. Phys. Fluids 22, 112103.

Sahu, K.C., Valluri, P., Spelt, P.D.M., Matar, O.K., 2007. Linear instability of pressure-driven channel flow of a Newtonian and Herschel–Bulkley fluid. Phys. Fluids 19, 122101.

Sameen, A., Govindarajan, R., 2007. The effect of wall heating on instability of channel flow. J. Fluid Mech. 577, 417–442.

Schäfer, P., Herwig, H., 1993. Stability of plane Poiseuille flow with temperature dependent viscosity. Int. J. Heat Mass Transfer 36, 2441–2448.

Schmid, P.J., Henningson, D.S., 2001. Stability and Transition in Shear FlowsSpringer, New York.

South, M.J., Hooper, A.P., 1999. Linear growth in two-fluid plane Poiseuille flow. J. Fluid Mech. 381, 121–139.

Sukanek, P.C., Goldstein, C.A., Laurence, R.L., 1973. The stability of plane channel flow with viscous heating. J. Fluid Mech. 57, 651–670.

Valluri, P., Naraigh, L.O., Ding, H., Spelt, P.D.M., 2010. Linear and nonlinear spatio-temporal instability in laminar two-layer flows. J. Fluid Mech. 656, 458–480.

Wall, D.P., Wilson, S.K., 1996. The linear stability of channel flow of fluid with temperature dependent viscosity. J. Fluid Mech. 323, 107–132.

Yiantsios, S.G., Higgins, B.G., 1988a. Linear stability of plane Poiseuille flow of two superposed fluids. Phys. Fluids 31, 3225–3238.

Yiantsios, S.G., Higgins, B.G., 1988b. Numerical solution of eigenvalue problems using the compound matrix-method. J. Comput. Phys. 74, 25.

Yih, C.S., 1967. Instability due to viscous stratification. J. Fluid Mech. 27, 337.